

2-18  
1973

"Made available under NASA sponsorship  
in the interest of early and wide dis-  
semination of Earth Resources Survey  
Program information and without liability  
for any use made thereof."

E7.3 1 0.4 6.1

CR-131261

LAND USE CLASSIFICATION USING TEXTURE INFORMATION  
IN ERTS-A MSS IMAGERY

K. Shanmugam, R.M. Haralick, Robert Bosley  
Remote Sensing Laboratory  
Center for Research, Inc.  
Space Technology Center  
2291 Irving Hill Drive - Campus West  
University of Kansas  
Lawrence, Kansas 66044

(E73-10461) LAND USE CLASSIFICATION  
USING TEXTURE INFORMATION IN ERTS-A MSS  
IMAGERY (Kansas Univ./Center for Research,  
Inc.) 30 p HC \$3.50  
CSCL 08B

N73-20419

Unclas

G3/13 00461

January 1973  
Technical Report  
Report No. 2262-1

Prepared for  
GODDARD SPACE FLIGHT CENTER  
Greenbelt, Maryland 20771  
(Contract No. NAS5-21822, Task No. 1)

Original photography may be purchased from:  
EROS Data Center  
10th and Dakota Avenue  
Sioux Falls, SD 57198

Report No. 2262-1	2. Government Accession No.	5. Report Date January 1973
4. Title and Subtitle Land Use Classification Using Texture Information in ERTS-A MSS Imagery		6. Performing Organization C
7. Author(s) K. Shanmugam, R.M. Haralick, Robert Bosley		8. Performing Organization Report No.
9. Performing Organization Name and Address Remote Sensing Laboratory Center for Research, Inc. University of Kansas 2291 Irving Hill Dr.-Campus West Lawrence, K		10. Work Unit No.
		11. Contract or Grant No. NAS5-21822
12. Sponsoring Agency Name and Address Goddard Space Flight Center Greenbelt, Maryland 20771 GSFC Technical Monitor: G.R. Stonesifer, Code 430		13. Type of Report and Period Covered Preliminary Technical Report
		14. Sponsoring Agency Code

15. Supplementary Notes

16. Abstract

The authors have identified the following significant results. Preliminary digital analysis of ERTS MSS imagery reveals that the textural features of the imagery are very useful for land use classification. A procedure for extracting the textural features of ERTS imagery is presented and the results of a land use classification scheme based on the textural features are also presented.

The land use classification algorithm using textural features was tested on a 5100 square mile area covered by part of an ERTS-A MSS band 5 image over the California coastline. The image covering this area was blocked into 648 subimages of size 8.9 square miles each. Based on a color composite of the image set, a total of 7 land use categories were identified. These land use categories are: coastal forest, woodlands, annual grasslands, urban areas, large irrigated fields, small irrigated fields, and water.

The automatic classifier was trained to identify the land use categories using only the textural characteristics of the subimages; 75 percent of the subimages were assigned correct identifications. Since texture and spectral features provide completely different kinds of information, a significant increase in identification accuracy will take place when both features are used together.

17. Key Words

Texture, land use classification, spatial processing

18. Distribution Statement

Unlimited

19. Security Class(this report)

none

20. Security Class. (this page)

none

*I*

21. No. of Pages

28

22. Price

3.50

## ABSTRACT

The authors have identified the following significant results. Preliminary digital analysis of ERTS MSS imagery reveals that the textural features of the imagery are very useful for land use classification. A procedure for extracting the textural features of ERTS imagery is presented and the results of a land use classification scheme based on the textural features are also presented.

The land use classification algorithm using textural features was tested on a 5100 square mile area covered by part of an ERTS-A MSS band 5 image over the California coastline. The image covering this area was blocked into 648 subimages of size 8.9 square miles each. Based on a color composite of the image set, a total of 7 land use categories were identified. These land use categories are: Coastal forest, woodlands, annual grasslands, urban areas, large irrigated fields, small irrigated fields, and water.

The automatic classifier was trained to identify the land use categories using only the textural characteristics of the subimages; 75 per cent of the subimages were assigned correct identifications. Since texture and spectral features provide completely different kinds of information, a significant increase in identification accuracy will take place when both features are used together.

# PRELIMINARY REPORT ON LAND USE CLASSIFICATION USING TEXTURE INFORMATION IN ERTS-A MSS IMAGERY

## I. INTRODUCTION

Two fundamental pattern elements used in human interpretation of pictorial data are texture and tone. The concept of tone is based upon varying shades of grey of resolution cells in the photographic image while texture is concerned with the spatial statistical distribution of grey tones. Much of the pattern recognition methods which have been used to process remotely sensed image data have been mainly concerned with temporal and spectral characteristics on a resolution cell level. Unfortunately such an approach does not take into account textural and context type information. Because the areal characteristics of texture and context carry so much information, it is important to develop appropriate pattern recognition features for them.

We describe in this report a procedure for determining the textural features on ERTS imagery. The textural features we have developed are extracted from the matrix of relative frequencies  $P_{ij}$  with which two neighboring resolution cells with a specific spatial relationship occur on the image, one with grey tone  $i$  and the other with grey tone  $j$ . Such matrices are calculated for each MSS image for different angular relationships between neighboring resolution cells as well as for different distances between them. From each of the different matrices, we extract features which contain information about the homogeneity of the image, linear dependencies in grey tone values, contrast and other image qualities and use these features for image classification.

Using the textural feature extraction-classification algorithm we have developed, we processed part of an ERTS MSS image over the California coast. We divided a 5400 square mile area on the image into 648 subimages each covering an area of approximately 8.5 square miles. The ground truth for the land use types for 629 of these images were obtained through photo-interpretation. The textural features were computed for 629 of the 648 subimages. Each subimage was then classified as belonging to one of seven possible land use categories using part of the data for training and the remainder of the data for testing the classification accuracy.

We found that over 70 per cent of the test samples can be correctly classified using the textural features of only one of the four MSS images. We conjecture that a much higher classification accuracy may be reached if the spectral information is used in addition to the textural features for all four MSS images in the set.

## II. TEXTURAL FEATURE EXTRACTION PROCEDURE

Other than some work with Fourier, Hadamard, and the autocorrelation function (Rosenfeld and Troy, 1970; Kaizer, 1955) there exists little or no theory to aid in establishing what the textural features should consist of. Rather, the feature extraction operation is determined intuitively, rationalized heuristically, and later justified pragmatically and empirically. For automatic analysis of MSS and other imagery we have developed a procedure to extract textural features from the spatial grey tone dependence matrix which is computed for each image.

### II.1 Spatial Grey Tone Dependence Matrix

Let  $L_x = \{1, 2, \dots, N_x\}$  and  $L_y = \{1, 2, \dots, N_y\}$  be the x and y spatial domains and  $L_y \times L_x$  be the set of resolution cells. Let  $G = \{0, 1, \dots, N_g\}$  be the set of possible grey tones. Then a digital image I is a function which assigns some grey tone to each and every resolution cell;  $I: L_y \times L_x \rightarrow G$ .\*

An essential component of our conceptual framework of texture is a matrix, or more precisely, four closely related matrices from which all texture-context features are derived. These matrices are termed angular nearest neighbor grey tone spatial dependence matrices.

We assume that the texture-context information in an image I is contained in the over-all or "average" spatial relationship which the grey tones in image I have to one another. More specifically, we shall assume that this texture-context information is adequately specified by the matrix of relative frequencies  $P_{ij}$  with

---

\*The spatial domain  $L_y \times L_x$  consists of ordered pairs whose components are row and column respectively. This convention conforms with the usual two subscript row-column designation used in FORTRAN.

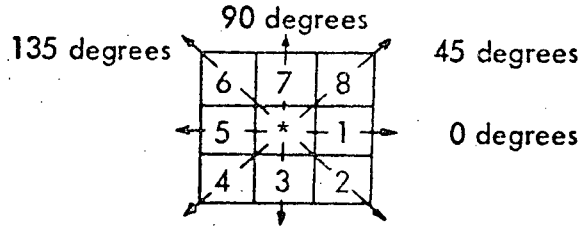


Figure 1. Resolution cells nos. 1 and 5 are the 0-degree (horizontal) nearest neighbors to resolution cell '\*', resolution cells nos. 2 and 6 are the 135-degree nearest neighbors, resolution cells 3 and 7 are the 90-degree nearest neighbors, and resolution cells 4 and 8 are the 45-degree nearest neighbors to '\*'. (Note that this information is purely spatial, and has nothing to do with grey tone values.)

which two neighboring resolution cells separated by distance  $d$  occur on the image, one with grey tone  $i$  and the other with grey tone  $j$  (see Figure 1). Such matrices of spatial grey tone dependence frequencies are a function of the angular relationship between the neighboring resolution cells as well as a function of the distance between them. Figure 2 illustrates the set of all horizontal neighboring resolution cells separated by distance 1. This set along with the image grey tones will be used to calculate a distance 1 horizontal spatial grey tone dependence matrix. Formally, for angles quantized to  $45^\circ$  intervals the unnormalized frequencies are defined by:

$$P(i, j, d, 0^\circ) = \# \{ ((k, l), (m, n)) \in (L_y \times L_x) \times (L_y \times L_x) \mid k-m=0, |l-n|=d, I(k, l)=i, I(m, n)=j \}$$

$$P(i, j, d, 45^\circ) = \# \{ ((k, l), (m, n)) \in (L_y \times L_x) \times (L_y \times L_x) \mid (k-m=d, l-n=-d) \text{ or } (k-m=-d, l-n=d), I(k, l)=i, I(m, n)=j \}$$

$$P(i, j, d, 90^\circ) = \# \{ ((k, l), (m, n)) \in (L_y \times L_x) \times (L_y \times L_x) \mid |k-m|=d, l-n=0, I(k, l)=i, I(m, n)=j \}$$

$$P(i, j, d, 135^\circ) = \# \{ ((k, l), (m, n)) \in (L_y \times L_x) \times (L_y \times L_x) \mid (k-m=d, l-n=d) \text{ or } (k-m=-d, l-n=-d), I(k, l)=i, I(m, n)=j \}$$

(1,1)	(1,2)	(1,3)	(1,4)
(2,1)	(2,2)	(2,3)	(2,4)
(3,1)	(3,2)	(3,3)	(3,4)
(4,1)	(4,2)	(4,3)	(4,4)

$$L_y = \{1, 2, 3, 4\}$$

$$L_x = \{1, 2, 3, 4\}$$

$$\begin{aligned}
R_H &= \left\{ (k,l), (m,n) \in (L_y \times L_x) \times (L_y \times L_x) \mid k-m=0, \mid l-n \mid = 1 \right\} \\
&= \left\{ (1,1), (1,2), (1,2), (1,1), (1,2), (1,3), (1,3), (1,2), \right. \\
&\quad (1,3), (1,4), (1,4), (1,3), (2,1), (2,2), (2,2), (2,1), \\
&\quad (2,2), (2,3), (2,3), (2,2), (2,3), (2,4), (2,4), (2,3), \\
&\quad (3,1), (3,2), (3,2), (3,1), (3,2), (3,3), (3,3), (3,2), \\
&\quad (3,3), (3,4), (3,4), (3,3), (4,1), (4,2), (4,2), (4,1), \\
&\quad \left. (4,2), (4,3), (4,3), (4,2), (4,3), (4,4), (4,4), (4,3) \right\}
\end{aligned}$$

Figure 2 illustrates the set of all distance 1 horizontal neighboring resolution cells on a 4 by 4 image.

Note that these matrices are symmetric;  $P(i, j; d, a) = P(j, i; d, a)$ . The distance metric  $\rho$  implicit in the above equations can be explicitly defined by  $\rho((k, l), (m, n)) = \max \{ |k-m|, |l-n| \}$ .

Consider Figure 3-a, which represents a 4 x 4 image with four grey tones, ranging from 0 to 3. Figure 3-b shows the general form of any grey tone spatial dependence matrix. For example, the element in the (2,1)-st position of the distance 1 horizontal  $P_H$  matrix is the total number of times two grey tones of value 2 and 1 occurred horizontally adjacent to each other. To determine this number, we count the number of pairs of resolution cells in  $R_H$  such that the first resolution cell of the pair has grey tone 2 and the second resolution cell of the pair has grey tone 1. In Figures 3-c through 3-f we calculate all four distance 1 grey tone spatial dependence matrices.

0	0	1	1
0	0	1	1
0	2	2	2
2	2	3	3

Figure 3-a.

		Grey Tone			
		0	1	2	3
Grey Tone	0	#(0,0)	#(0,1)	#(0,2)	#(0,3)
	1	#(1,0)	#(1,1)	#(1,2)	#(1,3)
	2	#(2,0)	#(2,1)	#(2,2)	#(2,3)
	3	#(3,0)	#(3,1)	#(3,2)	#(3,3)

Figure 3-b. This shows the general form of any grey tone spatial dependence matrix for an image with integer grey tone values 0 to 3. #(i,j) stands for number of times grey tones i and j have been neighbors.

$$0^\circ \quad P_H = \begin{pmatrix} 4 & 2 & 1 & 0 \\ 2 & 4 & 0 & 0 \\ 1 & 0 & 6 & 1 \\ 0 & 0 & 1 & 2 \end{pmatrix}$$

Figure 3-c.

$$90^\circ \quad P_V = \begin{pmatrix} 6 & 0 & 2 & 0 \\ 0 & 4 & 2 & 0 \\ 2 & 2 & 2 & 2 \\ 0 & 0 & 2 & 0 \end{pmatrix}$$

Figure 3-d.

$$135^\circ \quad P_{LD} = \begin{pmatrix} 2 & 1 & 3 & 0 \\ 1 & 2 & 1 & 0 \\ 3 & 1 & 0 & 2 \\ 0 & 0 & 2 & 0 \end{pmatrix}$$

Figure 3-e.

$$45^\circ \quad P_{RD} = \begin{pmatrix} 4 & 1 & 0 & 0 \\ 1 & 2 & 2 & 0 \\ 0 & 2 & 4 & 1 \\ 0 & 0 & 1 & 0 \end{pmatrix}$$

Figure 3-f.

The appropriate frequency normalization for these matrices can be easily computed.

## II.2 Textural Features

From each of the grey tone dependency matrices we extract a set of 32 textural features. The equations which define these features are given in Appendix A of this report. For illustrative purposes we define three of these features and explain their significance.

$$f_1 = \sum_{i=1}^{N_g} \sum_{j=1}^{N_g} \left( \frac{P(i,j)}{\#R} \right)^2,$$

$$f_2 = \sum_{n=0}^{N_g-1} n^2 \left\{ \sum_{|i-j|=n} \left( \frac{P(i,j)}{\#R} \right) \right\}$$

$$f_3 = \frac{\sum_{i=1}^{N_g} \sum_{j=1}^{N_g} \frac{ij P(i,j)}{\#R} - \mu_x \mu_y}{\sigma_x \sigma_y}$$

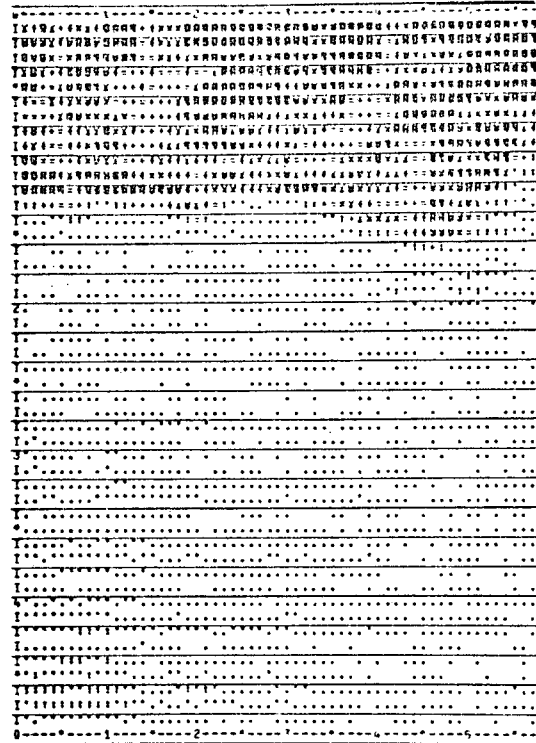
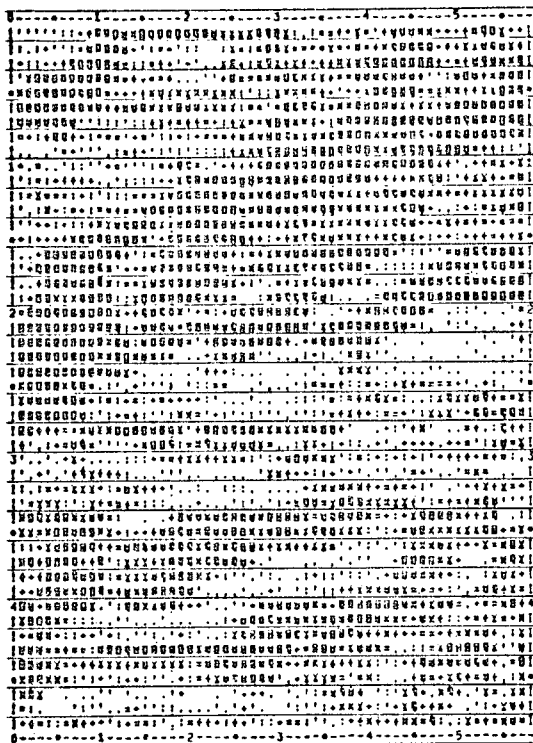
where

$\#R$  = number of resolution cells pairs, and  $\mu_x$  and  $\sigma_x$  are the mean and standard deviation of the marginal distribution  $P_x$  defined by

$$P_x(i) = \sum_{j=1}^{N_g} \frac{P(i,j)}{\#R}$$

and  $\mu_y$  and  $\sigma_y$  are the mean and standard deviation of the marginal distribution  $P_y$  defined by

$$P_y(j) = \sum_{i=1}^{N_g} \frac{P(i,j)}{\#R}$$



a. Grassland

b. Water Body

Angle	ASM	Contrast	Correlation	ASM	Contrast	Correlation
0°	.0128	3.048	.8075	.1016	2.153	.7254
45°	.0080	4.011	.6366	.0771	3.057	.4768
90°	.0077	4.014	.5987	.0762	3.113	.4646
135°	.0064	4.709	.4610	.0741	3.129	.4650
Avg.	.0087	3.945	.6259	.0822	2.863	.5327

Figure 4. Textural Features for Two Different Land Use Category Images.

To explain the significance of these features, let us consider the kind of values they take on two different land use category images. Figure 4 shows the digital printout of two sub-images of size  $64 \times 64$  resolution cells (approximately 8.5 square mile area) from MSS band 2 of the California frame. The image shown in 4(a) belongs to the grass land category and image shown in Figure 4(b) is mostly water. Values of the features  $f_1$ ,  $f_2$ , and  $f_3$  are also shown for these images in Figure 4.

The angular second moment features (ASM),  $f_1$ , is a measure of homogeneity of the image. In a homogeneous image, such as shown in 4(b), there are very few dominant grey tone transitions. Hence, the P matrix for this image will have fewer entries of large magnitude. For an image like the one shown in Figure 4(a), the P matrix will have a large number of small entries and hence the ASM feature which is the sum of squares of the entries in the P matrix will be smaller. A comparison of the ASM values given below the images in Figure 4 shows the usefulness of the ASM feature as a measure of the homogeneity of the image.

The contrast features,  $f_2$ , is obtained as a difference moment of the P matrix and is a measure of the contrast or the amount of boundaries present in an image. Since there is a large amount of boundaries present in the image 4(a) compared to the image shown in 4(b), the contrast feature for the grassland image has consistently higher values compared to the water body image.

The correlation feature,  $f_3$ , is a measure of linear grey tone dependencies in the image. For both the images shown in Figure 4, the correlation features is somewhat higher in the horizontal ( $0^\circ$ ) direction, along the line of scan. The water body image consists mostly of a constant grey tone value for the water plus some additive noise. Since the noise samples are mostly uncorrelated, the correlation features for the water body image have lower correlation values compared to the grassland image. Also the grassland image has a considerable amount of linear structure along  $45^\circ$  lines across the image and hence the value of the correlation feature is higher along this direction compared to the values for  $90^\circ$  and  $135^\circ$  directions.

The various features which we suggest are all functions of distance and angle. The angular dependencies present a special problem. Suppose image A has features  $a, b, c, d$  for angles  $0^\circ, 45^\circ, 90^\circ$ , and  $135^\circ$  and image B is identical to A except that B is rotated  $90^\circ$  with respect to A. Then B will have features  $c, d, a, b$  for angles  $0^\circ, 45^\circ, 90^\circ$ , and  $135^\circ$  respectively. Since the texture

context of A is the same as the texture context of B, any decision rule using the angular features  $a, b, c, d$  must produce the same results for  $c, d, a, b$  or for that matter  $b, c, d, a$  ( $45^\circ$  rotation) and  $d, a, b, c$  ( $135^\circ$  rotation). To guarantee this, we do not use the angularly dependent features directly. Instead, we use two symmetric functions of  $a, b, c, d$ , their average, and their range. These features can be represented in vector form  $F = [f_1, f_2, \dots, f_n]^T$ , where  $f_1, f_2, \dots, f_n$  are the values of the features,  $T$  denotes the transpose.

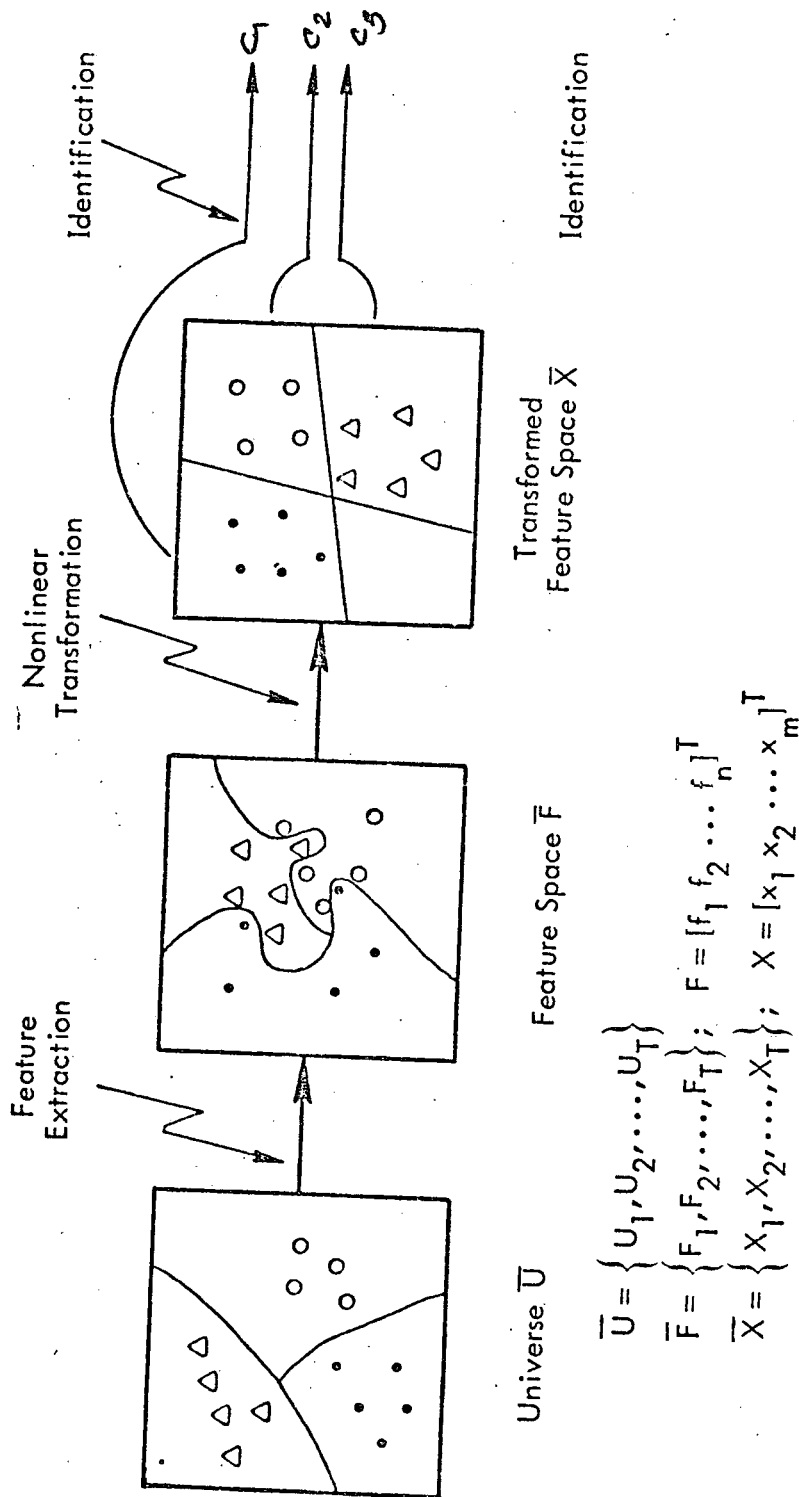
The textural features used in our study were computed for four angles and for a distance of one.

### III. IDENTIFICATION PROCEDURE

#### III.1 Introduction

The problem of developing procedures for categorizing environmental units consists of the following.

With reference to Figure 5, the universe  $\bar{U}$  consists of environmental units (for example rocks)  $U_1, U_2, \dots, U_T$  which belong to one of  $R$  possible categories  $C_1, C_2, \dots, C_R$  (different land use categories). Of the large number of environmental units present in the universe, we observe a smaller subset of units  $U_1, U_2, \dots, U_N$ . Our observations consist of a set of measured values of  $n$  features  $f_1, f_2, \dots, f_n$  for each unit  $U$  sampled. Based on the information contained in the feature vectors  $F_1, F_2, \dots, F_N$ , the categories of the environmental units which produce these measurements being known, we want to develop an algorithm to identify the categories of new units based on the measurements they produce.



The vectors  $F_i$  and  $X_i$  are usually referred to as feature vector and pattern vector respectively.

Figure 6. Identification Scheme.

The decision rule which assigns categories based on the values of features may be implemented in the feature space  $\bar{F}$  by partitioning  $\bar{F}$  into various regions and assigning categories to new units based on the regions to which their feature vectors belong. Efficient partitioning of the feature space may require complicated nonlinear decision boundaries (discriminant functions). Instead of deriving a decision rule in the feature space  $\bar{F}$ , we may transform the feature vectors into a new space  $\bar{X}$  and implement a decision rule in the new space  $\bar{X}$ . By using appropriate nonlinear transformations, we may be able to implement nonlinear decision boundaries in  $\bar{F}$  as linear decision boundaries in  $\bar{X}$ . Several procedures are available for deriving linear decision boundaries for partitioning  $\bar{X}$  into various regions, based on the information contained in a set of sample patterns  $X_1, X_2, \dots, X_N$  whose categories are known.

Identification Algorithms: In a widely used algorithm (Fukunaga 1972, Fu and Mendel 1970, Miesel 1972), the pattern space  $\bar{X}$  is separated into a number of regions using a set of hyperplanes (decision boundaries) whose locations are determined by the sample patterns. Each region is dominated by sample patterns of a particular category. When a new pattern is presented for identification, it is assigned a category depending on the region in which it belongs. If the new pattern  $X$  is located in a region dominated by sample patterns of category  $c_j$ , then  $X$  is classified as coming from category  $c_j$ .

To illustrate the procedure for obtaining the hyperplanes, consider the problem of separating the sample patterns  $X_1, X_2, \dots, X_{n_i}$  belonging to category  $c_i$  and  $X_{n_i+1}, X_{n_i+2}, \dots, X_{n_i+n_j}$  belonging to category  $c_j$ . We can write the linear discriminant function (hyperplane) which separates the patterns belonging to categories  $c_i$  and  $c_j$  as

$$\begin{aligned} h_{ij}(X) &= V_{ij}^T X + v_{ij}^0 \geq 0 \text{ for } X \in c_i, \\ h_{ij}(X) &= V_{ij}^T X + v_{ij}^0 < 0 \text{ for } X \in c_j \end{aligned} \quad (3)$$

The vector  $V_{ij}$  and the scalar  $v_{ij}^0$  are to be determined from the information contained on the sample patterns.

If we introduce a new form to express the pattern vectors as

$$\begin{aligned} Z &= [+1 \ x_1 \ x_2 \ \dots \ x_n]^T \text{ for } X \in c_i, \\ Z &= [-1 \ -x_1 \ -x_2 \ \dots \ -x_n]^T \text{ for } X \in c_j \end{aligned} \quad (4)$$

then the discriminant function can be written as

$$h_{ij}(Z) = W_{ij}^T Z \geq 0 \quad (5)$$

where  $W_{ij}$  is referred to as a weight vector and

$$h_{ij}(Z) = W_{ij}^T Z = 0 \quad (6)$$

is the equation of a hyperplane in the transformed feature space.

The weight vector  $W_{ij}$  is chosen so as to satisfy equation 5 for as many training patterns as possible. Usually we do not know the precise form of  $h_{ij}$ . But, given our knowledge of the categories of the training patterns, we can postulate reasonable values  $g_{ij}(Z_k)$  for  $h_{ij}(Z_k)$  and choose  $W_{ij}$  to minimize the mean square error given by

$$\epsilon^2 = \frac{1}{n_i + n_j} \sum_{k=1}^{n_i + n_j} (W_{ij}^T Z_k - g_{ij}(Z_k))^2 \quad (7)$$

Usually  $g_{ij}(Z_k)$  is taken to be +1 for  $k = 1, 2, \dots, n_i + n_j$ . We can rewrite  $\epsilon^2$  as,

$$\epsilon^2 = \frac{1}{(n_i + n_j)} [W_{ij}^T Y - G_{ij}^T] [Y^T W_{ij} - 1] \quad (8)$$

where  $Y = [Z_1 \ Z_2 \ \dots \ Z_{n_i + n_j}]$ , and

$$G_{ij} = [g_{ij}(Z_1) \ g_{ij}(Z_2) \ \dots \ g_{ij}(Z_{n_i + n_j})]$$

The weight vector which minimizes  $\epsilon^2$  given in equation 8 is given by

$$W_{ij} = (YY^T)^{-1} Y G_{ij} \quad (9)$$

which is the well-known normal equation set from linear least square theory.

For the multicategory problem involving  $N_R$  categories, a total of  $N_R(N_R - 1)/2$  hyperplanes must be determined using the procedure described above. After the hyperplanes are determined, the classification of new patterns is done as follows. For each category  $c_i$ , the number of hyperplanes,  $V_i$ , which give a positive response when the new pattern  $X$  is presented are determined using

$$V_i = \sum_{\substack{j=1 \\ j \neq i}}^{N_R} \frac{|W_{ij}^T Z| + W_{ij}^T Z}{2|W_{ij}^T Z|} ; i = 1, 2, \dots, N_R \quad (10)$$

where  $Z = \begin{bmatrix} 1 \\ X \end{bmatrix}$ .

$X$  is assigned to category  $c_j$  if

$$V_j = \max_i \{V_i\}$$

If there is a tie between categories  $c_m$  and  $c_n$ , then  $X$  is assigned to  $c_m$  if  $W_{mn}^T Z \geq 0$  or to  $c_n$  if  $W_{mn}^T Z < 0$ . Several modifications of the linear discriminant function method and a multitude of other classification procedures may be found in the references cited.

## IV. CLASSIFICATION EXPERIMENTS

### IV.1 MSS Data Used

All of the data used in our present study were derived from the MSS 5 band of ERTS-A image frame 1002-18134. The date of the flight was July 25, 1972, and the center coordinates of the frame were 37.291N, 120.935W. The area of coverage includes the San Francisco Urban area and the Monterey Bay on the coast line of California. Of the four image strips in this frame, all of strip one and one-half of strip three were digitally processed. The second MSS band image and the area processed are shown in Figure 6.

As a first step in the digital processing, the image was divided into a total of 648 sub-images of size 64 x 64 resolution cells (each covering a ground area of 8.5 square miles). For each of the sub-images, the digital spectral data from sensor band five (MSS band two) were extracted. The imagery data for each sub-image was then normalized using an equal probability quantizing algorithm and the 32 textural features for each sub-image were then computed.

Ground truth for each of the 648 sub-images were obtained with the help of photointerpreters working on the MSS images and the color composite image. A total of seven land use categories could be identified reasonably well and these categories are the following.

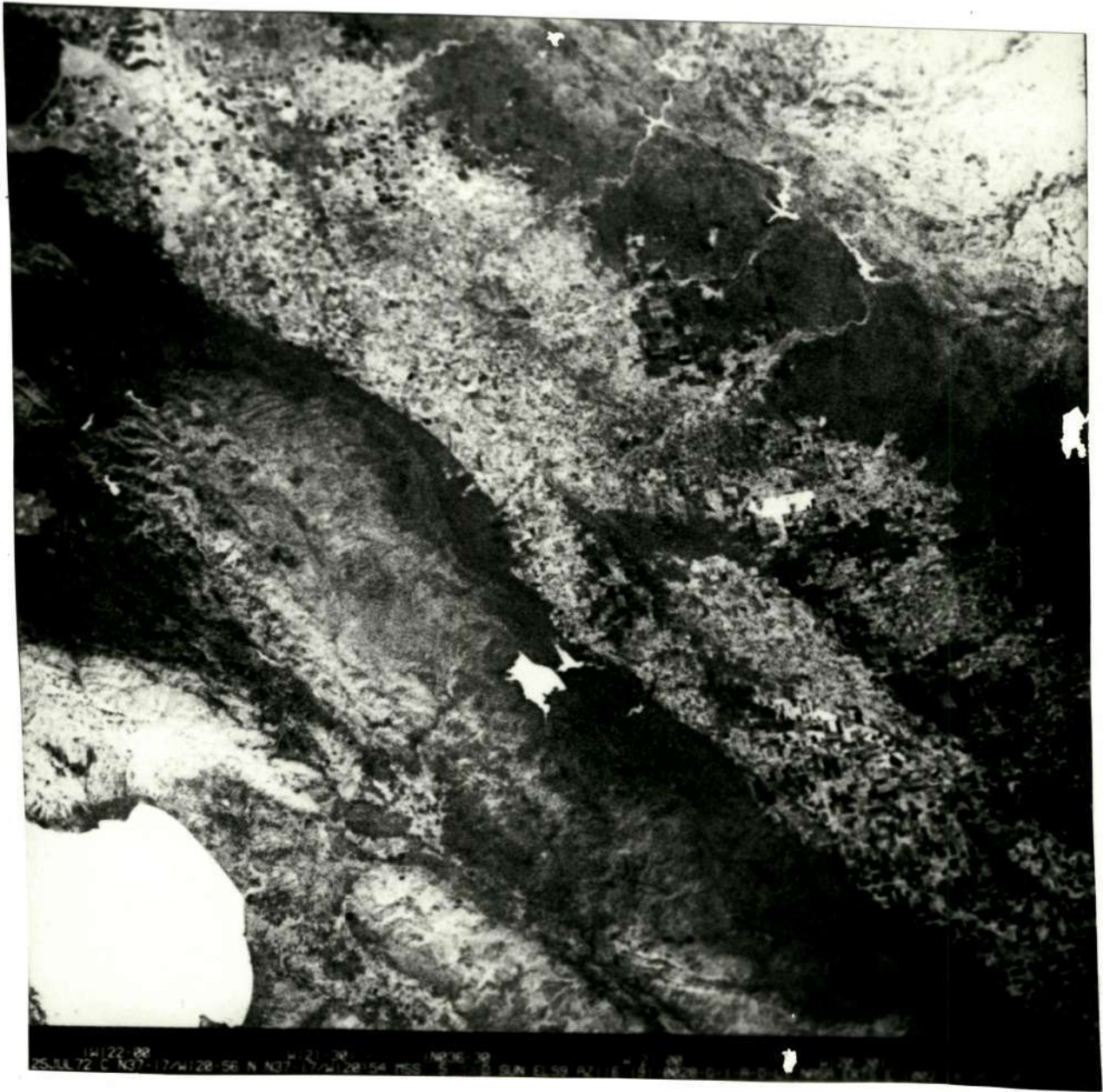
### IV.2 Categories of Land Use Detectable on ERTS Image (1002-18134)

#### (1) Coastal Forest

This area can be typified as a dense temperate rainforest sited on the windward side of the Coast Ranges of California. It is composed of needleleaf and broadleaf evergreen trees which generally form a continuous cover.

#### (2) Woodlands

These are areas to the leeward side of the Coast Ranges. At higher elevations, these woodlands consist of oaks, mostly evergreen, with varying but less continuous cover. At lower elevations these oak woods grade into chapparal which provides decreasing cover with decreasing elevation until it gives way to annual grasslands.



Reproduced from  
best available copy.

Figure 6. Two strips whose boundaries are shown on the top were processed from this MSS image set (1002-18134).

### (3) Annual Grasslands

This is an area of non-native annual grasses which have already completed their life cycle by the end of July (turned brown). This area is primarily, like the preceding two categories, quite mountainous. This is also the natural vegetation which would be found in the Great Valley of California except for anthropogenic vegetation.

### (4) Urban

Centers of human activity are extremely important as a landscape component within this frame they are none randomly located in a size hierarchy of central places connected by transport links. The primary urban agglomerations within the frame are the San Jose-Oakland segment of San Francisco, and parts of the Sacramento-Stockton urban complex. Unlike the preceding categories one of the main image features of urban areas is non-uniformity. Both pattern and texture, as well as a variety of tones, are associated with urban complexes.

### (5) Large Irrigated Fields

For practical purposes all field agriculture in the Great Valley is based on irrigation. The areas assigned to this category would most likely contain field crops such as cotton, alfalfa, and other crops readily adaptable to high mechanization. Most tree crops and vineyards would also be in this category.

### (6) Small Irrigated Fields

These areas would contain high value low mechanization crops typified by vegetables.

### (7) Water

Although almost self-explanatory as a term, the category in this instance is used to include: (1) ocean, (b) lakes - natural and man-made, and (c) standing water (in fields and on flood plains).

Out of the 648 sub-images in the frame, the photo-interpreters helped us to find a unique land use ground truth category for a total of 629 sub-images. Due to cloud cover and other ambiguities the ground truth for 19 sub-images could not be positively identified.

### IV.3 Results of Classification Experiments

The textural feature vectors for each of the 629 sub-images, for which ground truth was available, were divided arbitrarily into training and test sets. The classification algorithm was developed using the information contained in the training set and the samples in both the training and test set were assigned to one of the seven possible land use categories. The accuracy of classification was obtained by comparing the category assigned by the classifier with the ground truth category and the results are presented in the following paragraphs.

#### Experiment No. 1

The data set used in this experiment consisted of 416 sub-image samples obtained from strip 1 of the large image. There were six land use categories which could be identified on this image strip. These categories are: coastal forest; woodlands; annual grasslands; urban areas; water bodies; and large irrigated fields. Two classification tests were run on this data set. In the first classification run, 80 per cent or 334 of the 416 samples were used for training the classifier and the remaining 82 samples were used to test the accuracy of the classifier and up to 74.5 per cent of the test samples were classified correctly. The contingency table for this classification is given in Table 1.

In the second classification run, 70 per cent or 293 of the 416 samples were used for training. The accuracy of the classifier on the remaining 123 samples was found to be 68.5 per cent.

#### Experiment No. 2

All of the 629 sub-image samples for which the ground truth category can be identified were used in this experiment. There were seven ground truth categories, including the six categories used in the previous experiment and a small irrigated field category. Tests of the classifier were conducted using 80 per cent, 70 per cent, and 50 per cent of the samples respectively for training and the remaining samples for testing the classifier. A summary of the recognition accuracy of the classifier is given in Table 2.

TABLE 1  
CONTINGENCY TABLE FOR LAND USE CLASSIFICATION

Assigned Category True Category	Coastal Forest	Woodlands	Annual Grass- lands	Urban Area	Large Irrigated Fields	Small* Irrigated Fields	Water	Total
Coastal Forest	9	1	1	0	1	0	0	12
Wood- lands	1	7	0	0	2	0	0	10
Annual Grass- lands	0	2	15	2	1	0	0	20
Urban Area	0	2	4	4	0	0	0	10
Large Irrigated Fields	0	0	3	0	15	0	0	18
Small Irrigated Fields	0	0	0	0	0	0	0	0
Water	0	0	1	0	0	0	11	12
<b>Total</b>	<b>10</b>	<b>12</b>	<b>24</b>	<b>6</b>	<b>19</b>	<b>0</b>	<b>11</b>	<b>82</b>

Number of Training Samples = 334

Number of Test Samples = 82

Accuracy of Classification on Training Set = 86 per cent

Accuracy of Classification on Test Set = 74.5 per cent

\*There were no samples from small irrigated fields category in this data set.

**TABLE 2**  
**SUMMARY OF PERFORMANCE FOR VARIOUS TRAINING SET SIZES**

Percent of Samples Used for Training	80%	70%	50%
Accuracy of the Classifier on the Training Samples	78%	80.5%	90.5%
Accuracy of the Classifier on the Test Samples	72.5%	70.5%	67.5%

Details of classification for various land use categories for the 70 per cent training set are given in Table 4.

TABLE 3

## CONTINGENCY TABLE FOR LAND USE CLASSIFICATION OF TEST SAMPLES

Assigned Category True Category	Coastal Forest	Woodlands	Annual Grass- Lands	Urban Area	Large Irrigated Fields	Small Irrigated Fields	Water	Total
Coastal Forest	11	1	3	0	2	0	0	17
Woodlands	1	9	3	0	3	0	0	16
Annual Grasslands	0	2	61	3	5	0	1	72
Urban Area	1	1	8	4	0	1	0	15
Large Irrigated Fields	0	0	5	0	18	3	1	27
Small Irrigated Fields	0	0	10	0	1	10	0	21
Water	0	0	0	0	1	0	17	18
Total	13	13	90	7	30	14	19	186

Number of Training Samples = 443

Number of Test Samples = 186

Accuracy of Classification on Training Set = 80.5 per cent

Accuracy of Classification on Test Set = 70.5 per cent

## V. DISCUSSION

The overall accuracy of the automatic land use classification procedure based on the textural features of ERTS-A imagery is about 70 per cent. A substantial portion of the error in the classification procedure results from the classifier's inability to distinguish between the woodlands area and the annual grasslands, and the inability to correctly identify the urban areas. The difference in the textural characteristics of the woodlands area and the annual grassland is rather subtle since at lower elevations of the mountainous region the woodlands have decreasing cover until they give way to annual grasslands. The inability to correctly identify urban areas arise from the fact that urban areas have more than one type of texturally homogeneous areas and some of these areas look very much like other land use categories.

The accuracy of the classifier will be considerably improved if:

- (1) The textural features from all 4 MSS bands are used;
- (2) Some spectral characteristics are used as additional inputs to the classifier.

Experiments are currently underway to:

- (1) Obtain the comparative accuracy of a land use classification using spectral characteristics of the MSS data;
- (2) Use spectral characteristics as additional inputs to the classifier.

With a scheme using spectral and textural features we expect a significant improvement in the accuracy of the land use classification scheme. Further improvement in the accuracy of the classifier is possible if the sub-image samples are classified utilizing the probabilities of various categories occurring spatially adjacent to each other in the image. For example in the California frame, urban areas do not occur adjacent to large water bodies or irrigated fields. However, since the classifier assigns each sub-image to a land use category independent of the land use categories of the surrounding sub-images this context information is not utilized by the classifier. A compound decision rule can be developed to take into account this additional information and will lead to higher accuracy of classification.

## APPENDIX A

### TEXTURAL FEATURES OBTAINED FROM THE GREY TONE DEPENDENCE MATRIX

In this appendix, we define 16 textural features which are computed for each of the four angular grey tone dependence matrices. For each feature, we use the mean and range of the four values for the four angles, thus a total of 32 variables which are used as inputs to the classifier.

The following notation will be used in defining the 16 textural features.

$P(i, j)$  -  $(i, j)^{\text{th}}$  entry in a particular grey tone dependence matrix.

$\left. \begin{array}{l} \frac{P_x(i)}{\#R} \\ \frac{P_y(i)}{\#R} \end{array} \right\}$  -  $i^{\text{th}}$  entry in the marginal distributions of  $P(i, j)$  obtained by summing rows and columns of  $P(i, j)$  respectively.

$\#R$  - number of resolution cell pairs which were considered in computing the entries in  $P(i, j)$ .

$N_g$  - number of distinct grey tone values in the image.

$\mu$  - mean of  $P(i, j)/\#R$ .

$\frac{P_{x+y}(i)}{\#R}$  -  $i^{\text{th}}$  entry in the distribution of the sum of grey tones of neighboring resolution cells.

$\frac{P_{x-y}(i)}{\#R}$  -  $i^{\text{th}}$  entry in the distribution of the absolute differences in the grey tones of neighboring resolution cells.

## TEXTURAL FEATURES

### 1. Angular Second Moment:

$$f_1 = \sum_{i=1}^{N_g} \sum_{j=1}^{N_g} \left\{ \frac{P(i, j)}{\#R} \right\}^2 \quad (1)$$

### 2. Entropy:

$$f_2 = \sum_{i=1}^{N_g} \sum_{j=1}^{N_g} - \left( \frac{P(i, j)}{\#R} \right) \log \left( \frac{P(i, j)}{\#R} \right) \quad (2)$$

### 3. Correlation:

$$f_3 = \frac{\sum_{i=1}^{N_g} \sum_{j=1}^{N_g} ij \left\{ \frac{P(i, j)}{\#R} \right\} - \mu_x \mu_y}{\sigma_x \sigma_y} \quad (3)$$

where  $\mu_x$  and  $\sigma_x$  are the mean and standard deviation of  $P_x$ , and  $\mu_y$  and  $\sigma_y$  are the mean and standard deviation of  $P_y$ .

### 4. Sum of Squares on x:

$$f_4 = \sum_{i=1}^{N_g} \sum_{j=1}^{N_g} (i - \mu)^2 \left\{ \frac{P(i, j)}{\#R} \right\}$$

### 5. Product Moment:

$$f_5 = \sum_{i=1}^{N_g} \sum_{j=1}^{N_g} (i - \mu)(j - \mu) \left\{ \frac{P(i, j)}{\#R} \right\}$$

6. Inverse Moment:

$$f_6 = \sum_{i=1}^{N_g} \sum_{j=1}^{N_g} \frac{1}{1 + (i-j)^2} \left\{ \frac{P(i,j)}{\#R} \right\}$$

7. Difference Moment:

$$f_7 = \sum_{i=1}^{N_g} \sum_{j=1}^{N_g} (i-j)^2 \left\{ \frac{P(i,j)}{\#R} \right\}$$

8. Sum Average:

$$f_8 = \sum_{i=1}^{2N_g} i \left\{ \frac{P_{x+y}(i)}{\#R} \right\}$$

9. Sum Variance:

$$f_9 = \text{variance of } P_{x+y} / \#R$$

10. Sum Entropy:

$$f_{10} = \sum_{i=1}^{2N_g} - \left\{ \frac{P_{x+y}(i)}{\#R} \right\} \log \left\{ \frac{P_{x+y}(i)}{\#R} \right\}$$

11. Contrast:

$$f_{11} = \sum_{i=0}^{N_g-1} i^2 \left\{ \frac{P_{x-y}(i)}{\#R} \right\}$$

12. Difference Variance:

$$f_{12} = \text{variance of } \frac{P_{x-y}}{\#R}$$

13. Difference Entropy:

$$f_{13} = \sum_{i=0}^{N-1} - \left\{ \frac{P_{x-y}(i)}{\#R} \right\} \log \left\{ \frac{P_{x-y}(i)}{\#R} \right\}$$

14, 15, 16. Additional Measures of Correlation:

$$f_{14} = \frac{HXY - HXY1}{\max HX, HY}$$

$$f_{15} = \sqrt{1 - \exp[-2.0(HXY2 - HXY)]}$$

$$f_{16} = \sqrt{\text{second largest eigenvalue of } QQ^T}^*$$

where HX and HY are the entropies of the marginals of the transition matrix before quantization, HXY is the entropy of the transition matrix, and HXY2 is the entropy of the product distribution of the marginals before quantization;

$$Q(i, j) = P(i, j) / \sqrt{P_x(i)P_y(j)}$$

---

\*  $f_{16}$  is the maximal correlation coefficient.

## REFERENCES

1. Rosenfeld, A. and E. Troy, "Visual Textural Analysis," University of Maryland Computer Science Center, TR-70-116, June, 1970.
2. Kaizer, Herbert, "A Quantification of Textures on Aerial Photographs," Boston University Research Labs, Technical Note 121, 1955, AD69484.
3. Haralick, R. M. et al., "Texture-Tone Study with Application to Digitized Imagery," Technical Reports 182-2, 182-3, U. S. Army Engineer Topographic Laboratories Contract DAAK02-70-C-0388, University of Kansas Center for Research, Inc., 1971, 1972.
4. Fu, K. S. and J. M. Mendel, "Adaptive Learning and Pattern Recognition Systems," Academic Press, New York, 1972.
5. Miesel, W., "Computer Oriented Approaches to Pattern Recognition," Academic Press, New York, 1972.
6. Fukunaga, K., "Introduction to Statistical Pattern Recognition," Academic Press, New York, 1972.